Appl. Phys. A 79, 79–84 (2004)
DOI: 10.1007/s00339-003-2478-9

Applied Physics A
Materials Science & Processing

Invited paper

U. PAL[1,2]
J.F. SANCHEZ RAMIREZ[3]
H.B. LIU[1]
A. MEDINA[4]
J.A. ASCENCIO[1,✉]

Synthesis and structure determination of bimetallic Au/Cu nanoparticles

[1] Instituto Méxicano del Petroleo, Eje Central Lázaro Cárdenas 152, Col. San Bartolo Atepehuacan, C.P. 07730, México D.F., México
[2] Instituto de Física, Universidad Autónoma de Puebla, Apdo. Postal J-48, Puebla, Pue. 72570, México
[3] Facultad de Ciencias Quimicas, Universidad Autonoma de Puebla, 14 Sur, C.U. Puebla, Pue. 72570, México
[4] Instituto de Investigaciones Metalúrgicas, UMSNH, Edificio U. Ciudad Universitaria, Morelia, Michoacán 58000, México

Received: 5 November 2003/Accepted: 10 November 2003
Published online: 11 February 2004 •

ABSTRACT The synthesis of bimetallic nanoparticles has become so important in recent times due to its multi-faceted applications. The structure of the synthesised particles influences directly their properties. In this paper, we report the synthesis of Au/Cu nanoparticles by a simultaneous reduction method, considering three different molar concentrations (AuCu, $AuCu_3$ and Au_3Cu) of the components. In order to determine the size and structure of the obtained clusters, the particles were examined by optical spectroscopy, transmission electron microscopy and high-resolution transmission electron microscopy. One of the major factors, the minimum bimetal formation energy, was calculated by an embedded-atom method. The relation between the Au/Cu proportions has been demonstrated to affect the size of the particles and the corresponding structures. From the basic structural analysis it is found that the particles were fcc-like, multiple twin or multiple defect particles for the different Au/Cu concentrations. The smallest particles were identified for the Au/Cu sample with 50% of each, and the most crystalline structures were also obtained in the same sample.

PACS 61.46.+w; 61.16.-d; 31.15.Qg

1 Introduction

During the last decades, the development of new methods to synthesise nanoparticles with small size (< 3 nm), where the quantum properties become really important, have increased in number and variety, from physical to chemical based methods [1]. The impact of the nanoparticles is more if there is more than one element, as in the case of new nanostructured systems like Au/Ag [2] and particularly Au/Cu compound materials, which are focused to be used in catalysis [3], sensors [4], energy sources [5] and in many other applications. Bimetallic nanoparticles may be supported on matrices, for instance γ-alumina [3, 6] and Pt–C [7], where the two or more element composition induces better conditions in their use for fuel cells. Besides this, these systems have been demonstrated to be excellent materials for the refining processes in the petroleum industry, to produce fine chemicals [8] and also involving isomerisation of light petroleum fractions and naphtha reforming [9]. The main reasons for these materials to manifest their chemical selectivity and stability are their band gap and their electronic structures. This is directly related to both size [10, 11] and structure [12–14], which has been well supported on a theoretical basis [15] for small metal and semiconductor clusters. In the case of bimetallic clusters, this dependence of properties on their size and structure becomes critical, because of their atomistic structure. The distribution of elements in the composite particles influences their chemical and physical properties, which has a direct influence in the efficiency of device applications.

In order to determine the structure of small clusters, the uses of experimental techniques, together with theoretical [13–15] methods, have been demonstrated to be indispensable for an optimal interpretation of results and also for a better understanding of the structural implications in the corresponding properties for each possible configuration. One of the most used methods of characterisation is high-resolution transmission electron microscopy (HRTEM), mainly because of the possibility to obtain structural, chemical and morphological information from the same apparatus, and also at high precision.

Besides the structural information from the experimental characterisation, the use of molecular simulation methods allows one to understand (a) how the clusters are formed, (b) which atomistic distribution produces the minimal-energy configurations and (c) the most probable configuration in the real material. The calculation of the most favourable configuration, besides the HRTEM image simulation, generates the general scope of the structural conditions for the produced clusters and also for understanding the different properties produced with configurations such as the core–shell, solid solution or eutectic-like, which are the possible ones in these nanoparticles.

In this work, we report the production of small Au–Cu clusters by a relatively simple chemical method. Formation of the bimetallic particles was confirmed from TEM and optical absorption spectroscopy. Depending on the molar ratios of the component elements, the bimetallic particles of various structural configurations are produced. A complete structure determination of the bimetallic particles is done with the help of digital processing of the HRTEM images and molecular simulation techniques.

✉ Fax: +52-55/3003-6429, E-mail: ascencio@imp.mx

2 Methodology

2.1 *Synthesis of* Au/ Cu *clusters*

Colloidal dispersions of Au/Cu alloy nanoparticles were prepared under inert atmosphere by an improved simultaneous reduction method [16]. Solutions of tetrachloroauric acid (99.9% Aldrich, 0.033 mmol in 25 ml of methanol) were prepared by dissolving the crystalline material in methanol. Methanol solutions of copper (II) chloride (99.9% Aldrich, 0.033 mmol in 25 ml of methanol) were prepared in a similar way. Both the solutions were mixed at room temperature at various molar ratios to produce the mixture solutions containing poly(N-vinyl-2-pyrrolidone) (99.9% Aldrich, PVP, K-30, 300 mg, MW 10 000) as a protecting polymer. An extra 50 ml of methanol was added to the mixture solution to make a total volume of 100 ml to keep the total ion concentration in the mixture fixed. The mixture solutions were refluxed at about 50 °C for 1 h in nitrogen atmosphere. Then, an aqueous solution of $NaBH_4$ (3 ml of 0.022 M solution) was added to the resulting solution at 25 °C. A homogeneous colloidal dispersion in methanol was formed immediately after the addition of $NaBH_4$ solution to the mixture. For preparing the colloidal dispersions of the monometallic Au nanoparticles, 25 ml of PVP solution (150 g in 25 ml) was added to the methanol solution of $AuCl_2$ (0.033 mmol in 25 ml of methanol) and refluxed at about 50 °C for 1 h. Then, an aqueous solution of $NaBH_4$ (1.5 ml) was added to the resulting solution at 25 °C. The same procedure was used to prepare the monometallic Cu dispersions.

2.2 *Characterisation*

A Shimadzu UV-3101PC double-beam spectrophotometer with slit wavelength of 2 nm and light-path length of 1 cm was used to record the absorption spectra in the wavelength range 250–800 nm of the colloids. For transmission electron microscopic (TEM) observations, a drop of colloidal solution was spread on a carbon-coated copper microgrid and dried subsequently in vacuum. Two microscopes were used, a Jeol JEM200 for TEM observations at low magnification and a Tecnai 200 TEM with field-emission gun by FEI, with spherical aberration of 1 mm, minimal information limit of 0.15 nm and direct maximum resolution dot to dot of 0.23 nm, for high-resolution images respectively. HRTEM images were digitally processed by using filters in the Fourier space.

2.3 *Theoretical methods*

In order to identify the most stable configurations, interatomic interactions among Au/Cu were described by a simple analytical embedded-atom method (EAM) model developed by Cai and Ye [17]. The model includes a long-range force. In this model, the electron-density function is taken as a decreasing exponential function; a two-body potential is defined as a function as given by Rose et al. [18], and the embedding energy is assumed to be a universal form suggested by Banerjea and Smith [19]. The alloy model of Johnson [20] is applied and an extra parameter is introduced in order to fit dilute-limit heats of solution. For three possible compounds: $AuCu_3$, AuCu and Au_3Cu, the predicted heats of formation are in reasonable agreement with first-principles calculations and experimental data, and almost consistent lattice constants are predicted. That is, the Au–Cu alloying potential can apply in a wide range of components with great accuracy. The molecular dynamics simulations were performed using XMD developed by Prof. J. Riffkin, Center for Simulation, University of Connecticut [21]. The program employs a predictor–corrector algorithm to integrate the equation of motion. A time step of 5×10^{-15} s was used.

3 Results and discussion

Structural characteristics were studied from the experimental and theoretical observations and we have results in the directions that involve evidence of the main shapes known for pure metal particles and also related to the production, i.e. to the synthesis conditions.

3.1 *UV–Vis absorption spectra*

In order to identify the existence of possible Au and Cu metal states, the optical spectrometry measurements were carried out for monometallic and bimetallic clusters. Figure 1a shows the absorption spectra for three kinds of

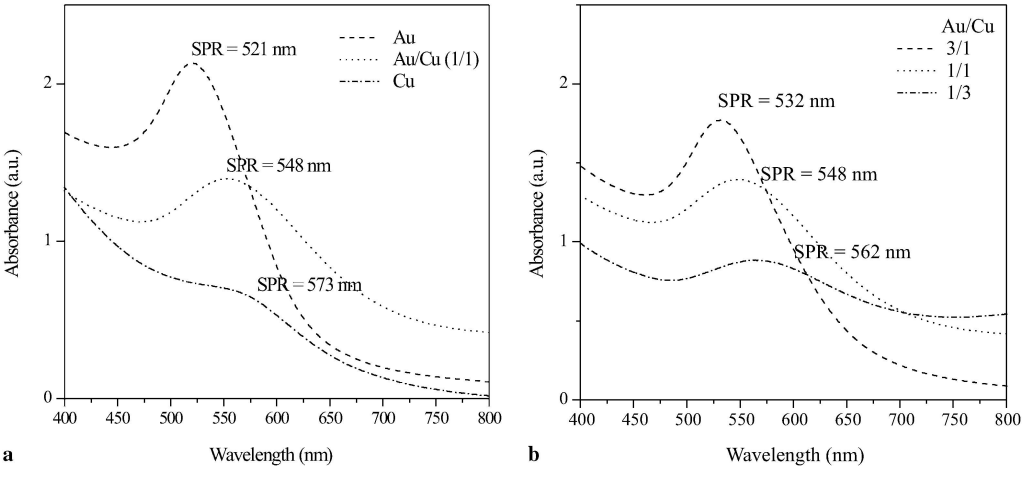

FIGURE 1 Absorption spectra. **a** The colloidal dispersions of monometallic Au, Au/Cu (1/1) alloy and monometallic Cu nanoparticles. **b** Au/Cu alloy colloids of three different ratios: 3/1, 1/1 and 1/3

samples; colloidal dispersions of monometallic Au, bimetallic Au/Cu alloy and monometallic Cu nanoparticles. The colloidal dispersion of monometallic Au exhibits a well-defined absorption peak at 521 nm, which is the absorption band spectra of nanometer-size metallic gold particles. The absorption band near 572 nm indicates the production of copper colloids, with size in the nanometer interval [22, 23]. For the dispersions of Au/Cu (1/1) bimetallic nanoparticles only a single SPR absorption band is revealed, and the peak position is different from the peak positions of monometallic Au and monometallic Cu nanoparticles. The absorption curve of the alloy dispersion could not be obtained by simple overlapping of the absorption curves of monometallic Au and monometallic Cu colloidal dispersions. We mention that the wavelength 548 nm (obtained for bimetallic alloy dispersions) is nearly the arithmetic mean value of 521 nm and 573 nm. Therefore, based on these spectra, it is reasonable to determine that the Au/Cu bimetallic nanoparticles are homogeneous alloy ones, the novel absorption band, 548 nm, for Au/Cu (1/1) is attributed to the SPR band of Au/Cu alloy nanoparticles and the composition of the alloy colloids is equal to the initial concentration of metal ions dissolved in methanol.

Besides, we produced the Au/Cu alloy colloids of arbitrary composition and found a linear relation between the SPR band positions in their absorption spectra and the composition of the constituents. Figure 1b shows the absorption spectra for three kinds of samples containing gold and copper of 3/1, 1/1 and 1/3 molar ratios. All three absorption curves are of Au/Cu alloys with different compositions. The maximum of the SPR absorption peak position is equal to the weighted mean of the wavelength of 521 nm for Au colloids and 573 nm for Cu monometallic colloids. For example, the calculated wavelength for Au/Cu (3/1) alloy colloids is 534 nm and the measured value is 532 nm. Similarly, they are 547 nm and 548 nm for Au/Cu (1/1) alloy colloids and 560 nm and 562 nm for Au/Cu (1/3) alloy colloids. Our X-ray- diffraction spectra of the bimetallic samples also revealed the formation of alloy structures [24, 25].

3.2 *Low-magnification transmission electron microscopy*

As one of the most important goals is to have control over the size of nanoparticles, we obtained several low-magnification images from the samples. The effects of the molar ratios and composition in the synthesis can be clearly observed in Fig. 2, which shows transmission electron micrographs with their corresponding size-distribution plots for each of the polymer-protected Au monometallic and Au/Cu = 3/1 and 1/1 bimetallic nanoparticles. From the figure, we can observe that the size of the monometallic Au particles is smaller than the average size of the bimetallic Au/Cu particles of 3/1 and 1/1 molar ratios. No coalescence or aggregation of particles is evident in the photographs, which must be because of the presence of polymer as a passivating agent. From the size-distribution histograms we can observe that there exists no evidence of a bimodal distribution, which suggests that the colloidal dispersion of bimetallic nanoparticles of Au/Cu obtained by this method is not a simple mixture

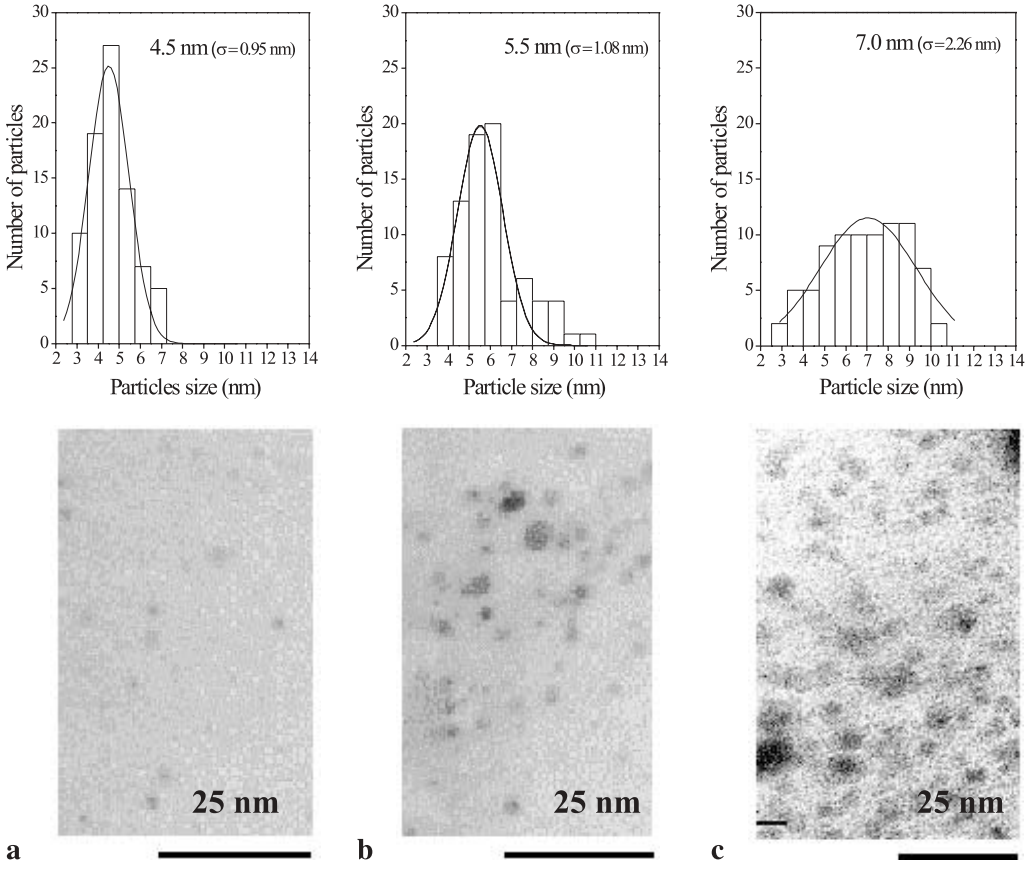

FIGURE 2 Transmission electron micrographs and particle size of the individual metallic and bimetallic nanoparticles: **a** Au, **b** Au/Cu (3/1) and **c** Au/Cu (1/1)

of monometallic nanoparticles of Au and Cu; rather, each of the particles consists of an alloy structure of the atoms of both Au and Cu. It is interesting to note that, on increasing the concentration of Cu ions in the mixture solution, the size and heterogeneity of the particle size increased. Our results suggest that the alloy particles are formed successfully and the bimetallic nanoparticles can be prepared with controlled size and homogeneity by controlling the concentration of two ions in the reaction mixture.

3.3 *Minimum-energy configurations*

For the embedded-atom model, the alloying pair potential determines the magnitude of chemical order. From Fig. 3, it can be seen that the Au/Cu alloying pair potential is very close to the mathematical average of Au/Au and Cu/Cu pair potentials, which indicates that the bimetal formation potential is very small and it should not affect the bimetal formation energy strongly. The other factor which may affect strongly the formation of bimetallic particles is structure incoherence. In fact, the nearest-neighbour distances in bimetallic Au–Cu alloys are different from those of pure Cu and Au by 11.4% and 12.8% respectively, which are large enough to generate a large structure incoherent energy. This is attributed to the contraction of the Au surface with the larger nearest-neighbour distance, leading to a good accommodation with the Cu core with the nearest-neighbour distance, which must induce the formation of nanoparticle shapes similar to the gold nanoparticles which are well studied, with both fcc-like and multiple twinned particles.

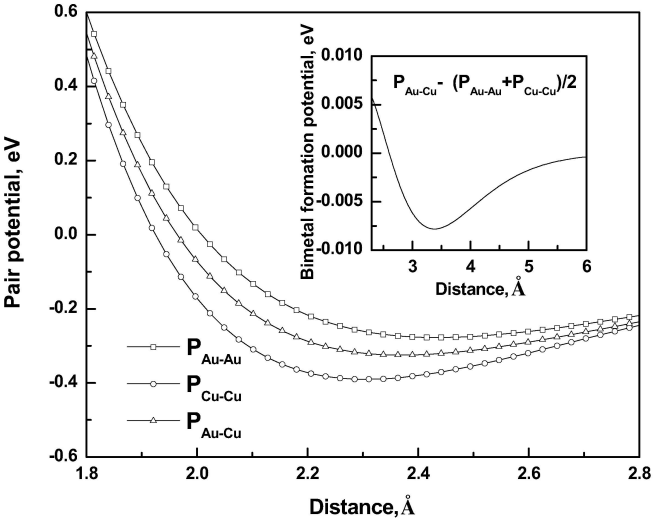

FIGURE 3 Pair potentials and bimetal formation potential for the Au–Cu system

3.4 *High-resolution transmission electron microscopy (HRTEM)*

In order to determine the structure of the synthesised nanoparticles, HRTEM images were obtained for the different samples. The analyses of shape, with their corresponding fast Fourier transforms, are shown in Figs. 4 and 5. These parameters have been demonstrated to be enough to distinguish both the structure and its corresponding orientation with respect to the electron-beam axis, as has been done in our previous report with the help of HRTEM simulation methods [13]. The description of the particles in this paper corresponds to the cubic, body-centred orthorhombic and rhombohedral notations for the fcc-like, decahedra and icosahedra respectively.

In Fig. 4, two HRTEM micrographs for the AuCu sample are presented. In both the images it is possible to distinguish several particles with different structures. In Fig. 4a, the FFT pattern for the whole image (T) shows the multiple reflections that denote several structures; while the three different marked shapes generate significant differences between them. A well-defined square array is obtained from the particle I, which clearly is associated with a fcc-like cluster with the {0, 0, 1} orientation. A hexagonal pattern is identified for the particle II, which also shows a dot splitting that is characteristic of twins or defects in the crystalline order, so that this particle can be associated with a single twin cluster, while in the last particle (III) the FFT pattern shows two main reflections with

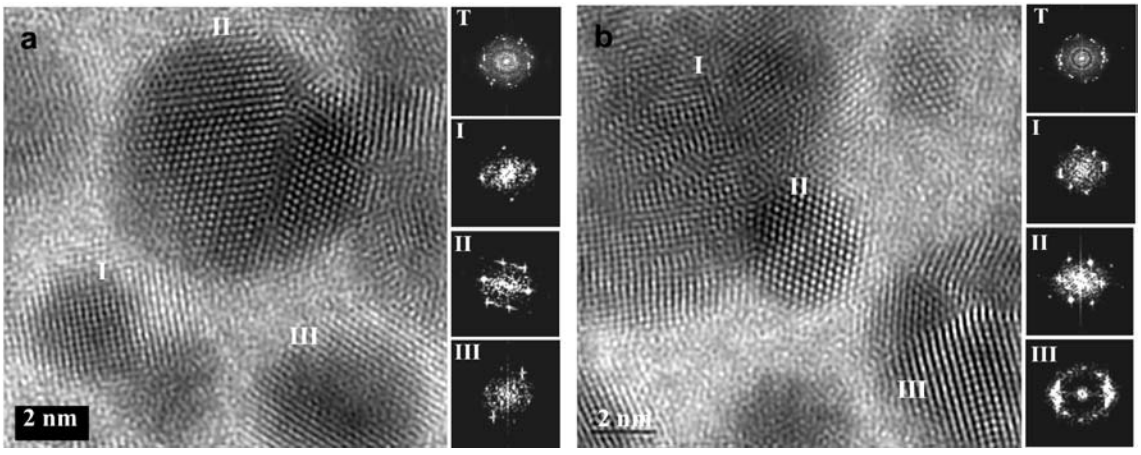

FIGURE 4 HRTEM images of nanoparticles from AuCu samples. **a** The image shows three particles with their corresponding FFTs and the total (T), an fcc-like particle at {0, 0, 1} orientation (I), a single twin particle (II) and an fcc-like particle at {0, 0, 1} orientation (III). **b** A couple fcc-like nanoparticles are shown at {0, 0, 1} and {0, 1, 1} orientations (I and II respectively) besides a decahedral particle III

low-intensity extra dots that are directly associated with a fcc-like particle rotated to be oriented near to the {1, 1, 1} axis. In Fig. 4b, a similar analysis allows us to determine the existence of two fcc-like particles in the {0, 0, 1} and {0, 1, 1} orientations for the particles I and II respectively, while the particle III corresponds to a decahedron particle near to the {0, 0, 1} orientation. These particles are common in the AuCu samples, as well as some other configurations in lower quantity.

In Fig. 5, HRTEM images of five particles of the $AuCu_3$ sample are presented. The difference of this sample from the AuCu sample is very clear in the images. In this case, we can observe the formation of multiple twin particles, corresponding to almost all the observed clusters. From the particles shown in Fig. 5, it is possible to distinguish an icosahedron particle at the {0, 0, 1} orientation in Fig. 5a, while Fig. 5b shows a decahedron structure rotated by 15° from the five-fold axis (with respect to the electron beam). The three images, Fig. 5c–e, correspond to multiple defect particles (mdp), particularly in the case of the image presented in Fig. 5e, which shows clearly that these defects are formed in three dimensions, even producing moiré, which are noticed in the FFT pattern in the internal dots. So, the mdp clusters are common in the sample.

Finally, Fig. 6 shows the images of particles from the Au_3Cu sample. In this case, the clusters tend to have well-defined configurations including the fcc-like particles, as is shown in Fig. 6a for a truncated octahedron at the {0, 1, 2} orientation. In Fig. 6b, a single twin particle is observed, while Fig. 6c corresponds to a decahedron particle at the five-fold axis, where the five twins are easily distinguished. Figure 6d and e correspond to two icosahedra at the five-fold and $\{1, -1, 2\}$ orientations respectively.

Because of the multiple kinds of structures identified for each sample, a plot of the structure distribution in the samples is shown in Fig. 7, where more than 100 particles were used for each sample. The percentage of particles is plotted for the cubic-like (fcc), single twin (stwin), decahedra (deca), icosahedra (ico) and multiple defect particles (mdp) for each corresponding sample. It is clear that the main particles for the AuCu sample have well-ordered structures, such as the fcc-like and decahedra while, for the $AuCu_3$ sample, the multiple defect particles correspond to almost 50% of the total, and the majority are multiple twin configuration (deca, ico and mdp). Finally, for the case of the Au_3Cu sample, the influence of Au is significant and it affects the structure; the most common configurations include a regular distribution of particles for

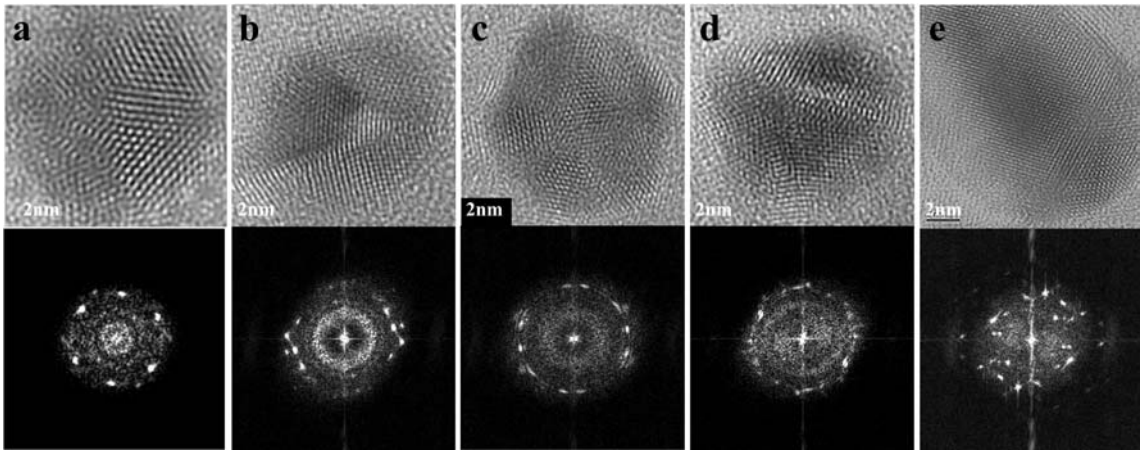

FIGURE 5 HRTEM images of nanoparticles with their corresponding FFTs from $AuCu_3$ samples. **a** Icosahedral particle at the {0, 0, 1} orientation, **b** decahedron near to the five-fold axis. The three images **c**, **d** and **e** correspond to multiple defect particles

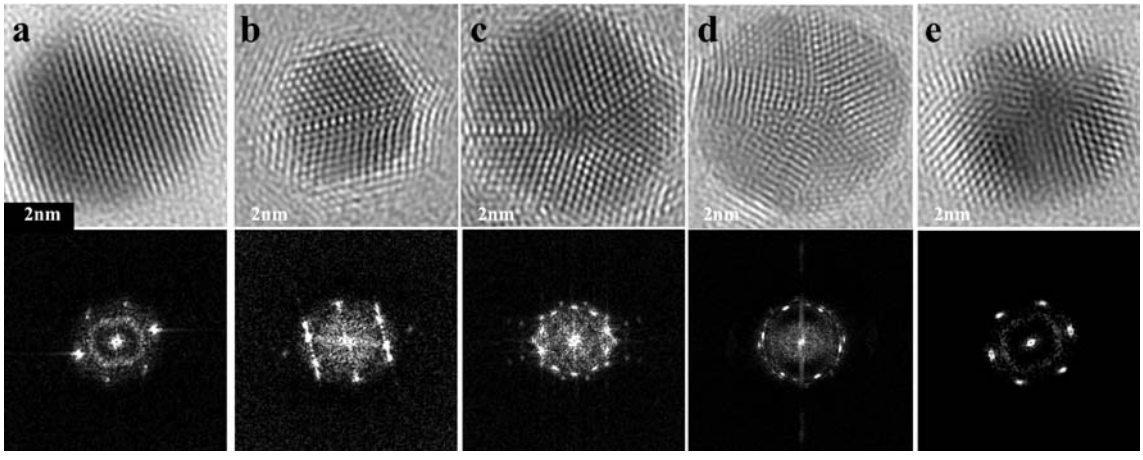

FIGURE 6 HRTEM images of nanoparticles with their corresponding FFTs from Au_3Cu samples. **a** Truncated octahedron at the {0, 1, 2} orientation, **b** single twin cluster, **c** decahedron at the {0, 0, 1} orientation and two icosahedron nanoparticles at the five-fold and $\{1, -1, 2\}$ orientations in the images (**d**) and (**e**) respectively

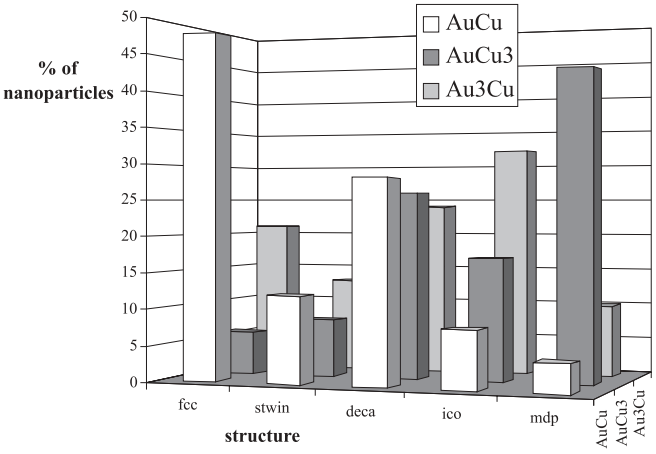

FIGURE 7 Plot of nanoparticle frequencies for the identified structures for the different Au/Cu concentrations

the three main structures, fcc-like, decahedra and icosahedra, as many authors have reported for small metal particles.

From the different analytical data and theoretical results we can relate the synthesis conditions to the size and structure of the obtained particles. In this way, the influence of the element concentrations defines the production of preferential arrays, while a higher Au concentration in the bimetallic clusters produces more ordered structures.

4 Conclusions

Using the simple synthesis method reported in this work, it is possible to produce small bimetallic particles with different structures. The concentration of elements in the synthesis directly affects the size and structure of the obtained clusters, producing the smallest and the most crystalline particles for the AuCu samples while, for the $AuCu_3$ synthesised particles, we obtained the largest clusters with a higher quantity of defects and with a strong influence of the Au atoms in the synthesis. This configuration for the sample obtained with the higher quantity of Au atoms over the Cu ones (Au_3Cu) is common to the single-element metallic clusters. The energy analysis also allows us to identify the metal configurations as a function of the structure, producing similar effects to the single-element metallic small particles. In this way, it is possible to conclude a high influence of the gold concentration on the bimetal formation potential and the surface energy, which affects directly the shape and stability of the obtained clusters, producing more multiple twin configurations when the Au concentration is higher, and more defects without well-defined structure when the Cu concentration is higher. We must indicate that the crystalline structures proposed for these alloys agree with the obtained nanoparticles in the interplanar spacing but the effect of surface-energy minimisation involved a tendency to produce more spherical clusters with fcc-like, multiple twinned and also structures with a high quantity of defects due to a strong internal stress and a high formation energy when the Cu elements dominate the cluster composition. We suggest that a more rigorous study is necessary to understand the details of the local atomistic distribution in the particles, and in this paper we conclude that there is evidence of the influence of the element concentration in the production of their preferential shapes.

REFERENCES

1 M. José-Yacamán: Metall. Mater. Trans. **29A**, 713 (1998)
2 S. Link, C. Burda, Z.L. Wang, M.A. El-Sayed: J. Chem. Phys. **11**, 1255 (1999)
3 M. José-Yacamán, J.A. Ascencio, S. Tehuacanero, M. Marin: Top. Catal. **18**, 167 (2002)
4 A. Ruiz, J. Arbiol, A. Cirera, A. Cornet, J.R. Morante: Mater. Sci. Eng. C **19**, 105 (2002)
5 R.J. De Meijer, C. Stapel, D.G. Jones, P.D. Roberts, A. Rozendaal, W.G. Macdonald, K.Z. Chen, Z.K. Zhang, Z.L. Cui, D.H. Zuo, D.Z. Yang: Nanostruct. Mater. **8**, 205 (1997)
6 Y.M. Cheng, H.K. Rhee: Catal. Lett. **85**, 159 (2003)
7 P. del Angel, J.M. Dominguez, G. del Angel, J.A. Montoya, J. Capilla, E. Lamy-Pitara, J. Barbier: Top. Catal. **18**, 183 (2002)
8 P. Fouilloux: in *Heterogeneous Catalysis and Fine Chemicals*, ed. by M. Guisnet (Elsevier, Amsterdam 1998) p. 123
9 N.Y. Chen, T.F. Degnan: Chem. Eng. Prog. **32**, 88 (1988)
10 S.K. Shaikhutdinov, R. Meyer, M. Naschitzki, M. Bäumer, H.-J. Freund: Catal. Lett. **86**, 211 (2003)
11 M. José-Yacamán, J.A. Ascencio, H.B. Liu: J. Vac. Sci. Technol. B **19**, 1091 (2001)
12 L. Guczi, D. Horvath, Z. Paszti, G. Peto: Catal. Today **72**, 101 (2002)
13 J.A. Ascencio, C. Gutiérrez-Wing, M.E. Espinosa-Pesqueira, M. Marín, S. Tehuacanero, C. Zorrilla, M. José-Yacamán: Surf. Sci. **396**, 349 (1998)
14 G.A. Somorjai, Y.G. Borodko: Catal. Lett. **76**, 1 (2001)
15 A. Samanta, S.K. Ghosh: Chem. Phys. Lett. **349**, 483 (2001)
16 Y. Wang, H. Liu, N. Toshima: J. Phys. Chem. **100**, 19 533 (1996)
17 J. Cai, Y.Y. Ye: Phys. Rev. B **54**, 8398 (1996)
18 J.H. Rose, J.R. Smith, F. Guinea, J. Ferrante: Phys. Rev. B **29**, 2963 (1984)
19 A. Banerjea, J.R. Smith: Phys. Rev. B **37**, 6632 (1988)
20 R.A. Johnson: Phys. Rev. B **39**, 12 554 (1989)
21 J. Riffkin: Center for Simulation, University of Connecticut, USA [http://ims.uconn.edu/centers/simul]
22 J.S. Bradley, E.W. Hill, C. Klein, B. Chaudret, A. Duteil: Chem. Mater. **5**, 254 (1993)
23 J.S. Bradley, G.H. Via, L. Bonneviot, E.W. Hill: Chem. Mater. **8**, 1895 (1996)
24 S. Link, M. El-Sayed: J. Phys. Chem. B **103**, 8410 (1999)
25 F. Gonella, G. Mattei, P. Mazzoldi, C. Sada, G. Battaglin, E. Cattaruzza: Appl. Phys. Lett. **75**, 55 (1999)